Ore Geology Reviews 64 (2015) 387–399

Contents lists available at ScienceDirect

Ore Geology Reviews

journal homepage: www.elsevier.com/locate/oregeorev

Fluid inclusions, muscovite Ar–Ar age, and fluorite trace elements at the Baiyanghe volcanic Be–U–Mo deposit, Xinjiang, northwest China: Implication for its genesis

Xiaofeng Li [a,*], Guo Wang [b], Wei Mao [a], Chunzeng Wang [c], Rong Xiao [d], Mou Wang [b]

[a] State Key Laboratory of Ore Deposit Geochemistry, Institute of Geochemistry, Chinese Academy of Sciences, Guiyang 550002, China
[b] No. 216 Geological Survey, China National Nuclear Corporation, Urumqi 830011, China
[c] University of Maine at Presque Isle, Presque Isle, ME 04769, USA
[d] Hunan Institute of Geological Survey, Changsha 410116, China

ARTICLE INFO

Article history:
Received 4 May 2014
Received in revised form 22 July 2014
Accepted 23 July 2014
Available online 30 July 2014

Keywords:
Be–U–Mo mineralization
Fluorite
Fluid inclusions
Fluid mixing
Muscovite Ar–Ar dating
Pb isotope
Baiyanghe deposit
Northwest China

ABSTRACT

The Baiyanghe Be–U–Mo deposit is located in the Late Paleozoic Xuemisitan–Kulankazi island arc of the northwestern margin of the Junggar plate, Northwest China. It is the largest Be deposit (2.2 M tons of ore with grades ranging from 0.2% to 1.4%) in Asia. Orebodies in the deposit occur as fractures along contact zones between the Yangzhuang granite porphyry intrusion and Devonian pyroclastic country rocks and within the porphyry itself. Muscovite–fluorite veins are closely associated with the Be–U–Mo mineralization. A new Ar–Ar dating of the muscovite in this study yields a plateau age of 303.0 ± 1.6 Ma, which constrains the timing of the Be–U–Mo mineralization of the deposit. Three stages of fluorite of different colors have been identified at the deposit, with the earliest dark-purple fluorite more closely associated with the mineralization. Microthermometry of fluid inclusions obtained from the three stages of fluorite suggests that the fluorites were precipitated as veins from low temperature (120–150 °C) hydrothermal fluids with salinity ranging from 4.7 to 19.7 wt.% NaCl eqv. Based on the trace elemental concentrations and REE patterns of the fluorite, the style of veining, and the low salinity and low temperature characters of the fluid inclusions, it is suggested that Be and U were most likely transported as fluoride complexes and Mo as hydroxyl complexes. Pb isotopic compositions of the ores and country rocks, as well as O and H isotopic characters of the ore-related muscovite, indicate mixing between magmatic and meteoric waters; both contributed to formation of the ore-forming fluids. Metallic Be, U, and Mo were most likely leached out from the granite porphyry by the fluids. The fluid mixing led to the reduction of U, Mo, and Be and their precipitation at the deposit.

1. Introduction

The Baiyanghe Be–U–Mo deposit is located in the Late Paleozoic Xuemisitan–Kulankazi island arc of the northwestern margin of the Junggar plate, Northwest China (Fig. 1) (Dong et al., 2010; Wang and Tang, 1997; Tang and Wang, 1998). The deposit occurs within contact zones between the Yangzhuang granitic porphyry intrusion and Devonian pyroclastic country rocks. The deposit has three types of ores, namely U type, Be type, and Be–U–Mo type (Wang et al., 2012; Xiao et al., 2011; Xiu et al., 2011). The U type ore was first discovered by No. 519 Geological Survey of CNNC (China National Nuclear Corporation) in 1956. The high-concentration BeO samples were found by the Xinjiang Geological Bureau in 1975. At that time, it was considered to be a topaz rhyolitic type Be–U deposit. Extensive surface exploration and drilling by the No. 216 Geological Survey of CNNC since 2006 has yielded ore reserves up to 2.2 M metric tons with BeO grades ranging from 0.2% to 1.4%. The deposit is thus rated as the largest Be deposit in Asia. Zou (2006) compared the Baiyanghe Be–U–Mo deposit with the F-rich U–Be deposit of Spor Mountain of the United States (Lindsey, 1977) and suggested that the Baiyanghe Be–U–Mo deposit was hydrothermal in origin and formed after the emplacement of the Yangzhuang granite porphyry. Multistage fluorite observed in the deposit was indicative of a multistage Be–U–Mo mineralization at the Baiyanghe deposit (Fayek and Shabaga, 2011; Mao et al., 2013). However, the mineralization age and genesis of the Baiyanghe Be–U–Mo deposit and its relation to the Yangzhuang granite porphyry remain unclear. To address these issues, the present authors conducted systematic analysis of fluid inclusions and trace elements of fluorite, Ar–Ar geochronology of muscovite, and O and H isotopes of muscovite. New analyses, results, and findings are reported in this paper.

* Corresponding author at: Institute of Geochemistry, Chinese Academy of Sciences, 46 Guanshui Road, Guiyang, Guizhou 550002, China. Tel.: +86 18811080229.
E-mail address: x-f-li@hotmail.com (X. Li).

http://dx.doi.org/10.1016/j.oregeorev.2014.07.017
0169-1368/

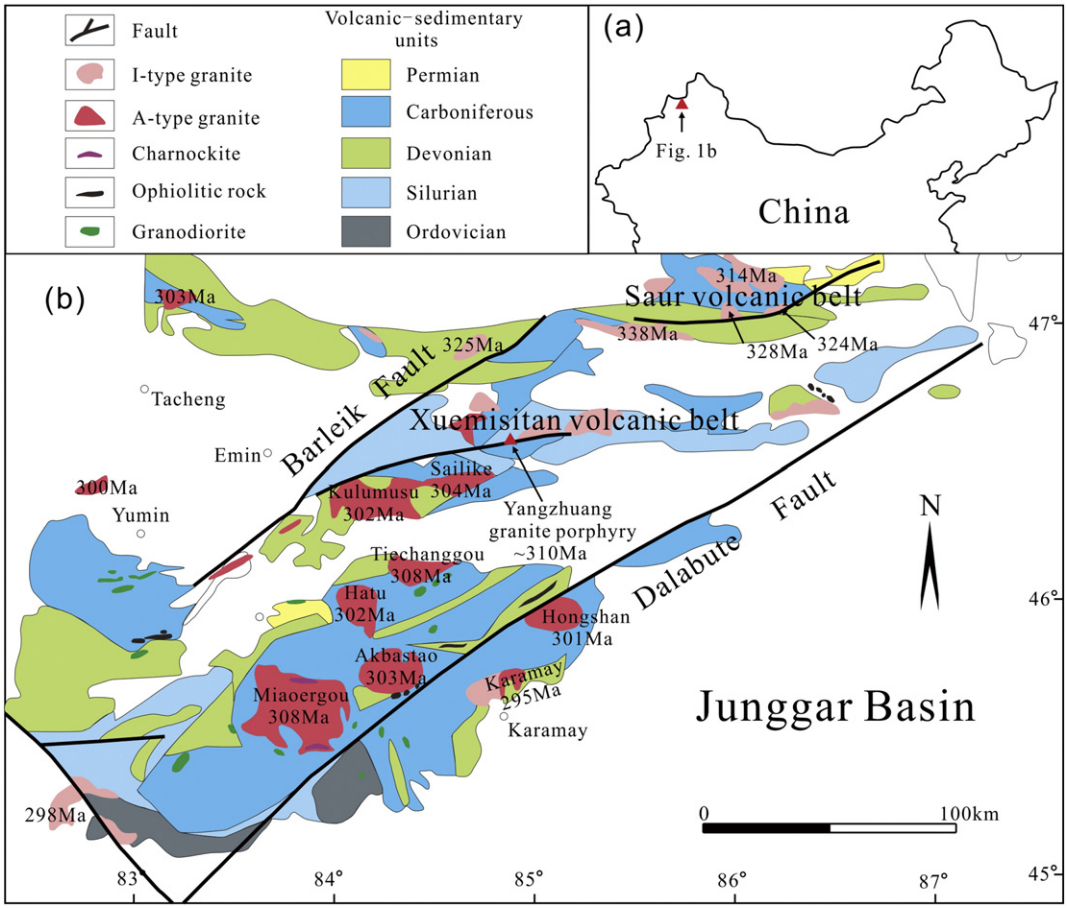

Fig. 1. Simplified geologic map of the Western Junggar, Xinjiang, northwest China (modified after Chen et al., 2010).

2. Geological setting

The Baiyanghe deposit is located at the junction of the Tarim, Kazakhstan, and Siberian plates. The area is characterized by three magmatic belts: the EW-trending Xuemisitan volcanic belt, the EW-trending Saur volcanic belt, and the NE-trending alkali–feldspar granite belt (Chen et al., 2010) (Fig. 1). The Xuemisitan volcanic belt resulted from southward subduction of the Junggar oceanic crust during the Late Silurian–Early Devonian. The belt is dominated by a suite of Devonian intermediate to felsic volcanic and intrusive rocks, with minor amounts of Late Carboniferous–Middle Permian granite, granite porphyry, and diorite.

The Baiyanghe Be–U–Mo deposit occurs on the northwestern margin of the Xuemisitan volcanic belt. Stratigraphic sequences in the Baiyanghe area include the Late Devonian Tarbagatay Group of intermediate-felsic volcanic and pyroclastic rocks with minor mafic tuff, the Early Carboniferous Hebukehe Group of shale, limestone, siliceous shale, sandstone and conglomerate, and the Early Carboniferous

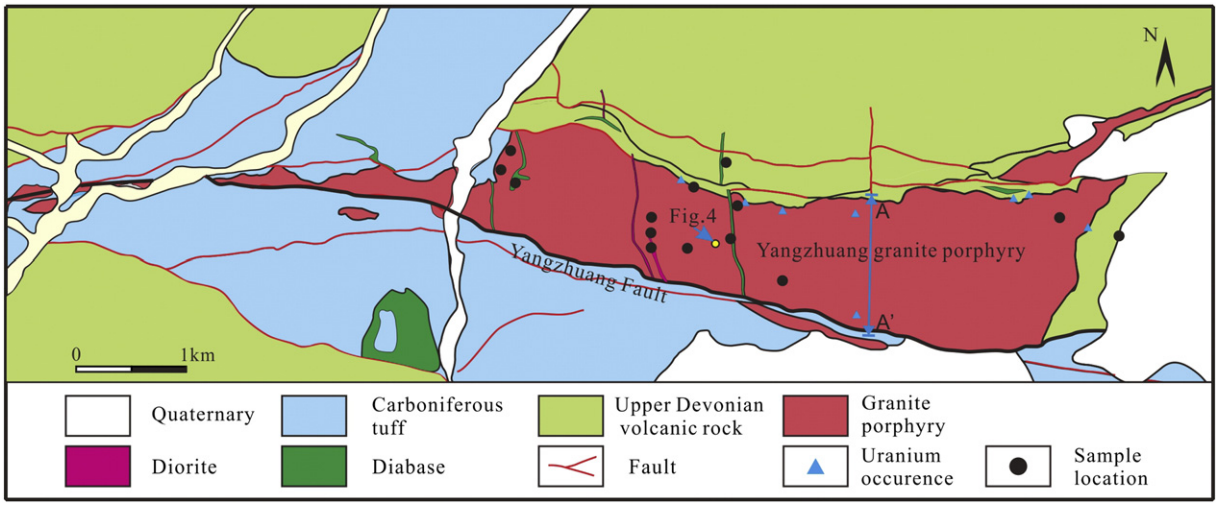

Fig. 2. Simplified geological map of the Baiyanghe Be–U–Mo deposit (modified after Wang et al., 2012).

Heishantou Group of mafic-intermediate volcanic and pyroclastic rocks (Mao et al., 2013; Wang et al., 2012; Zhang and Zhang, 2014). NW–SE trending diabase and diorite dikes that intrude into the Late Carboniferous Yangzhuang granite porphyry are widely developed (Fig. 2) (Mao et al., 2014).

The Baiyanghe Be–U–Mo mineralization is mainly related to the Yangzhuang granite porphyry. It was intruded along the EW-trending Yangzhuang Fault in the south and the Devonian volcanic rocks in the north and the east. The contact zone is curved between the Yangzhuang granite porphyry and the Devonian volcanic rocks and dips south at an angle of 32°. The Yangzhuang Fault contact between the Yangzhuang granite and the Upper Carboniferous rocks dips north at an angle of 45°–75°.

The Yangzhuang granite porphyry exhibits a porphyritic texture with 3–8% quartz and K-feldspar phenocrysts. Anhedral quartz and slightly altered euhedral feldspar phenocrysts are identified under the microscope. The matrix is composed of microcrystalline quartz, K-feldspar, plagioclase and minor amounts of biotite. The accessory minerals were mostly magnetite with hematitization. Zircon U–Pb dating of the Yangzhuang granite porphyry yielded an intrusion age of ~310 Ma (Ma et al., 2010; Mao et al., 2014; Zhang and Zhang, 2014).

3. Geology of the Baiyanghe Be–U–Mo deposit

The Baiyanghe Be–U–Mo deposit is hosted by the Yangzhuang granite porphyry (Fig. 2). Be–U–Mo ore bodies mainly occur in fractures along contact zones between the Yangzhuang granite porphyry and its country rocks and also inside the porphyry itself (Fig. 3). Three types of ores are identified in the deposit, namely U type, Be type, and U–Be–Mo type (Wang et al., 2012; Xiao et al., 2011; Xiu et al., 2011). These three types of ores occur either separately or show a cross-cutting relationship (Fig. 4). The Be–U–Mo mineralization is spatially associated with the intrusion of the NW-trending diabase dikes. The diabase dikes are dull green in color, and their width varies from a few centimeters to several meters within the Yangzhuang granite porphyry. It has about 63–64% plagioclase, 20–25% augite, 5–10% hornblende and 1–2% quartz. The accessory minerals in the diabase are mostly magnetite with lesser apatite. The area in the western section of the porphyry, where the diabase and diorite dikes are well developed, has a lower Be–U grade. However, in the eastern section, the diabase and diorite dikes are scarcer and have a higher Be–U grade.

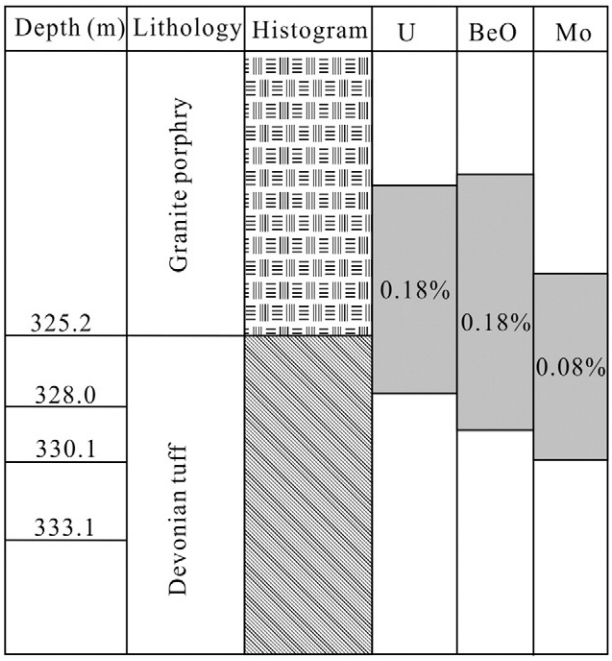

Fig. 4. Histogram of drill hole (ZK3612) showing Be, U, and Mo orebodies and the relationship between U, Be, and Mo mineralization.

Three Be–U orebodies have been identified to date. The No. 1 orebody is the largest and contains 90% BeO reserves (Fig. 3). The No. 1 orebody is present as a stratiform in the contact zone. It is 600 m long horizontally, and extends up to 300 m in depth at a dip of 32°. Its thickness ranges from 1.5 m to 20.2 m with an average of 5.1 m. The gangue minerals are quartz, albite, K-feldspar, sericite, chlorite, and fluorite. The primary U-bearing mineral is pitchblende, and the secondary U-bearing mineral is uranophane. The Be-bearing mineral is bertrandite, which mainly occurs as fine planar and 20–300-μm-long prismatic crystals within the dark purple fluorite veins.

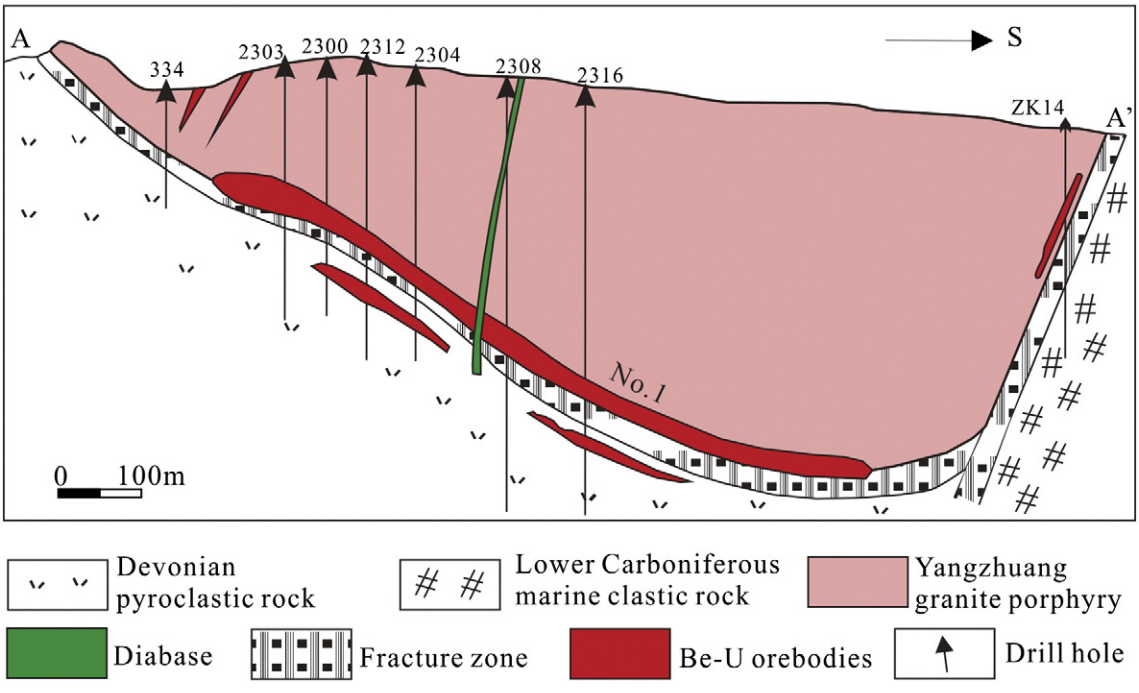

Fig. 3. Cross-section of the Baiyanghe U–Be–Mo deposit showing Be–U–Mo mineralization.

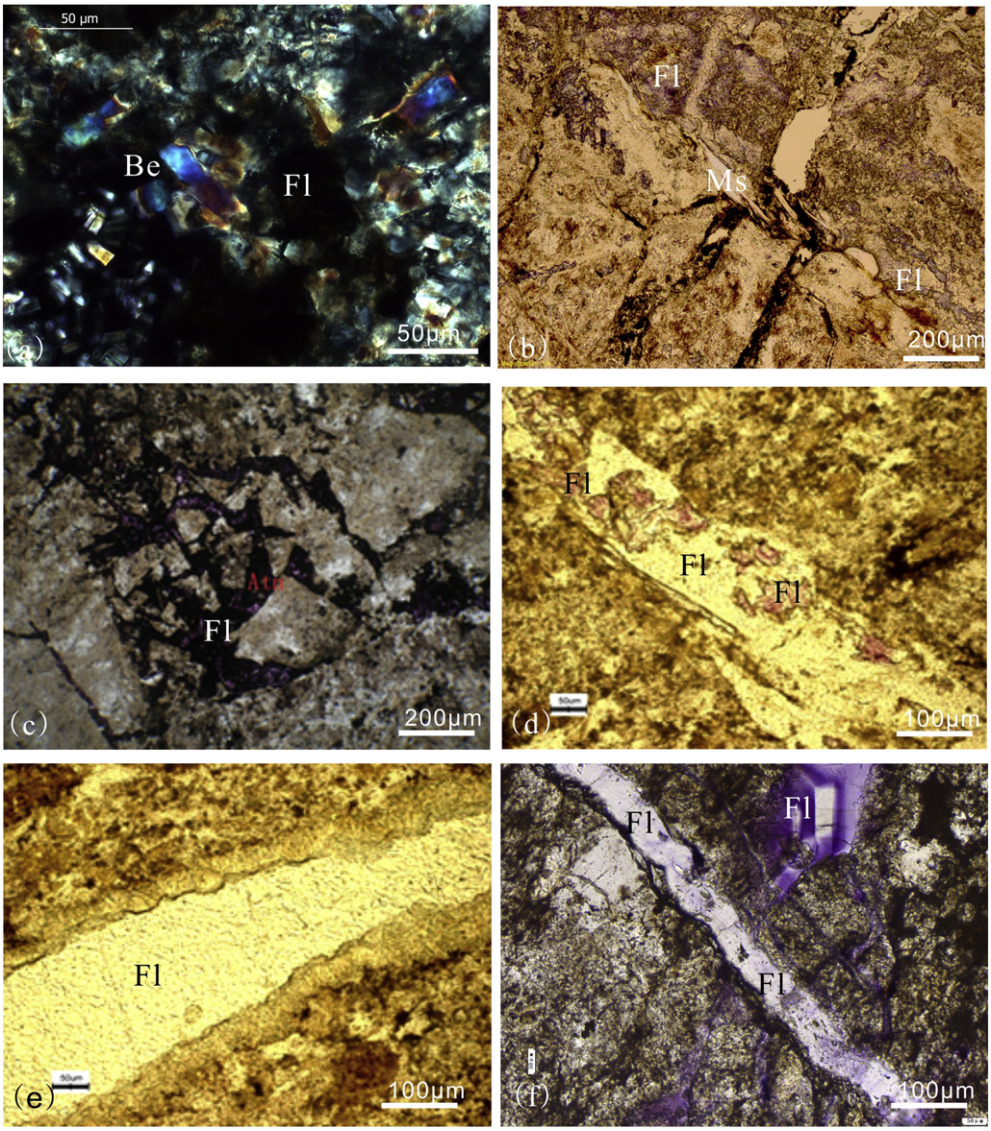

Fig. 5. Representative photomicrographs show the relationship between fluorite veins in different colors and muscovite alteration with bertrandite. (a) Bertrandite (Be) is associated with purple fluorite (Fl) in an ore sample; (b) Muscovite (Ms) occurs as a veinlet with fluorite (Fl) in U ore sample; (c) Dark-purple fluorite occurs in fractures within the Late Devonian glassy tuff; (d) Purple fluorite occurs as disseminated in green fluorite within rhyolitic ignimbrite tuff; (e) White fluorite vein in rhyolitic ignimbrite tuff; (f) Zoned purple fluorite vein is cross-cut by younger white fluorite vein in tuff.

Table 1
Sample descriptions from the Baiyanghe deposit, northwest China.

Samples	Mineral	Description
ZK46-1	Colorless fluorite	Colorless vein in tuff; from drill hole ZK4610 at depth of 15 m
ZK46-2	Colorless fluorite	Colorless vein in tuff; from drill hole ZK4610 at depth of 20 m
ZK60-1	Green fluorite	Green fluorite vein of 2–3 mm wide within the granite porphyry; from drill hole ZK60-1 at depth of 15 m
ZK13-1	Green fluorite	Green fluorite vein of 2–3 mm wide in tuff; from drill hole ZK13101-1 at depth of 205.6 m, with some pale purple fluorite within the vein
ZK13-5	Green fluorite	Green fluorite + zoning purple fluorite vein within granite porphyry; from drill hole ZK13101-2 at depth of 376.3 m
ZK13-3	Zoning fluorite	Green fluorite + zoning purple fluorite vein within granite porphyry; from drill hole ZK13101-2 at depth of 376.3 m
ZK13-6	Pale purple fluorite	Green fluorite vein in tuff; from drill hole ZK13101-4 at depth of 205.6 m, with some pale purple fluorite in the vein
BY12-58	Dark-purple fluorite	Muscovite + dark-purple fluorite + bertrandite vein
ZK1432-1	Dark-purple fluorite	Dark-purple fluorite vein in granite porphyry; from drill hole ZK1432-1 at depth of 16 m
ZK4612-3	Dark-purple fluorite	Dark-purple fluorite vein in granite porphyry; from drill hole ZK4612-3 at depth of 356.5 m
BY12-13	Calcite	Calcite vein within diabase dike at an outcrop
BY12-15	Calcite	Calcite vein within diabase dike at an outcrop
ZK6026-4	Calcite	Calcite vein from drill hole at depth of 200 m
ZK6022-1	Calcite	Calcite vein within diorite dike; from drill hole ZK6022-1 at depth of 211 m
ZK13101-5	Calcite	Calcite vein within tuff; from drill hole ZK13101-5 at depth of 211 m
BH-1	Muscovite	Muscovite + dark-purple fluorite + bertrandite vein
BY12-29	Muscovite	Muscovite + deep-purple fluorite + bertrandite vein
BY12-58	Muscovite	Muscovite + dark-purple fluorite + bertrandite vein
ZK6026-7	Muscovite	Altered granite porphyry
ZK13101-3	Muscovite	Altered granite porphyry

Hydrothermal alteration minerals observed in the ores include hematite, fluorite, quartz, chlorite, and muscovite (Wang et al., 2012). Field and microscopic observations show that the fluorite, hematite, and muscovite are closely associated with Be–U–Mo mineralization (Fig. 5).

Fluorite shows white, green, and dark-purple colors in the Baiyanghe deposit (Fig. 5). The earliest-stage fluorite is generally the best developed, is dark-purple or purple in color, has a mottled texture, and coexists with U-, Be-, and Mo-bearing minerals. The younger green fluorite occurs in miarolitic cavities and veins and may contain schlieren-like or zoned inclusions of the earliest-stage dark-purple fluorite (Fig. 5d). Colorless (or white) fluorite veins of the youngest stage may cross-cut the older fluorites (Fig. 5f). All fluorite veins may be cross-cut by much younger calcite veins or stained by hematite (Mao et al., 2013).

4. Sampling and analytical methods

4.1. Sample description

Thirteen whole rock samples (including the Yangzhuang granite porphyry, diabase, diorite and Devonian rhyolite and basalt), 3 ore samples, 10 fluorite samples of different stages, two hydrothermal muscovite samples from muscovite + fluorite + bertrandite veinlets within the Be–U ores, and two muscovite samples from altered granite porphyry that were collected from drill cores and outcrops. Detailed sample descriptions are given in Table 1. The muscovite samples were used for Ar–Ar dating and O and H isotopic analysis. The fluorite samples were used for fluid inclusion analysis and trace elemental analysis. The whole rock samples and ore samples were used for Pb isotopic analysis.

4.2. Muscovite Ar–Ar dating

The muscovite sample BH-1 collected from a Be–U-mineralized fluorite vein was purified using a magnetic separator and then cleaned by ultrasonic treatment with ethanol. The purity of the muscovite grains (at a size of 0.08–0.15 mm) is greater than 99%. The muscovite grains were irradiated for 51 h in a nuclear reactor at the Chinese Institute of Atomic Energy in Beijing and subsequently cooled for approximately 100 days. $^{40}Ar/^{36}Ar$ stepwise heating analysis was performed at the Institute of Geology, Chinese Academy of Geological Sciences, using a MM-1200B Mass Spectrometer. Measured isotopic ratios were corrected for the mass discrimination, atmospheric Ar component, blanks and irradiation induced mass interference. The decay constant used is $d = 5.543 \pm 10^{-10}$ year^{-1} (Steiger and Jager, 1977). All ^{37}Ar analyses were corrected for radiogenic decay (half-life = 35.1 days). Uncertainty in each apparent age is given at 2σ. The monitor used in this analysis was an internal standard: Fangshan biotite (ZBH-25) of 132.7 Ma, which has a potassium content of 7.6%. The J-values of the

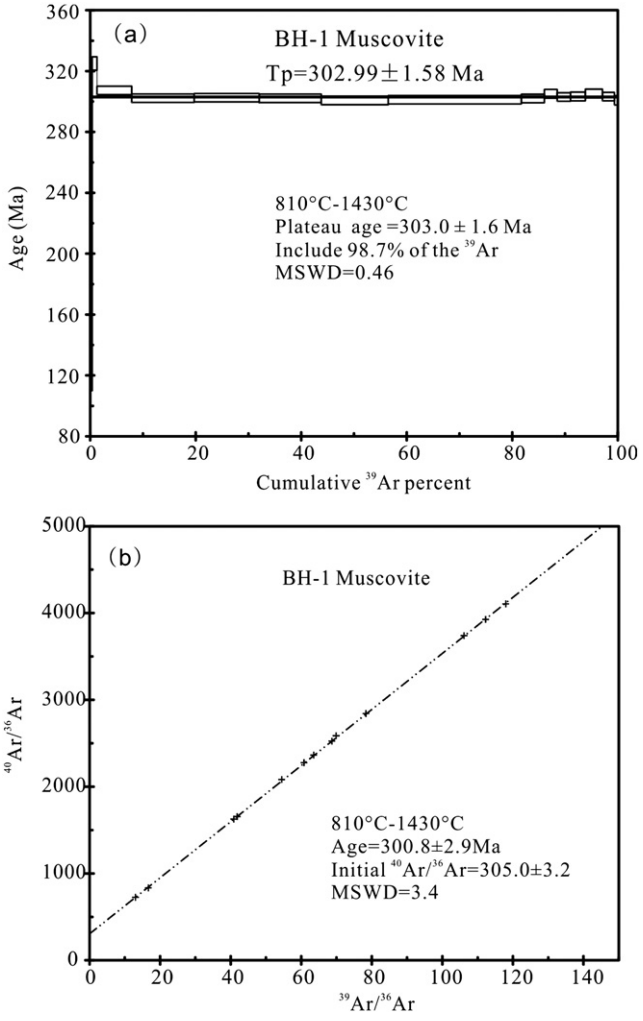

Fig. 6. Apparent $^{40}Ar/^{39}Ar$ age spectra for the dated muscovite.

Table 2
$^{40}Ar/^{39}Ar$ step-heating data of muscovite from the Baiyanghe deposit, northwest China.

T (°C)	$(^{40}Ar/^{39}Ar)_m$	$(^{36}Ar/^{39}Ar)_m$	$(^{37}Ar/^{39}Ar)_m$	$(^{38}Ar/^{39}Ar)_m$	^{40}Ar (%)	F	^{39}Ar ($\times 10^{-14}$ mol)	^{39}Ar (Cum.) (%)	Age (Ma)	±1σ (Ma)	Ca/K
700	2253.5911	7.5703	0.0000	1.4567	0.74	16.5721	0.16	0.38	161	51	0
750	263.4406	0.7726	0.3003	0.1615	13.34	35.1493	0.38	1.30	325.0	4.4	0.5177
810	55.7566	0.0768	0.0130	0.0283	59.29	33.0611	2.74	7.89	307.3	2.8	0.0224
860	39.5651	0.0239	0.0000	0.0179	82.13	32.4717	4.92	19.72	302.2	2.8	0
900	36.2754	0.0128	0.0000	0.0156	89.59	32.4994	5.12	32.04	302.5	2.8	0
940	35.2459	0.0094	0.0009	0.0152	92.08	32.4562	4.89	43.80	302.1	2.8	0.0016
980	34.8032	0.0085	0.0290	0.0153	92.79	32.2940	5.28	56.50	300.7	2.8	0.05
1020	34.9823	0.0089	0.0179	0.0151	92.46	32.3459	10.49	81.72	301.2	2.8	0.0309
1060	36.7466	0.0146	0.0658	0.0164	88.28	32.4423	1.82	86.10	302.0	2.8	0.1134
1100	37.0426	0.0143	0.0152	0.0157	88.57	32.8079	1.00	88.51	305.1	2.9	0.0262
1160	37.2145	0.0157	0.0256	0.0166	87.49	32.5591	1.05	91.03	303.0	2.8	0.0441
1240	37.4623	0.0165	0.0000	0.0161	87.01	32.5960	1.17	93.85	303.3	2.9	0
1320	38.2563	0.0184	0.0000	0.0162	85.81	32.8280	1.35	97.09	305.3	2.9	0
1400	39.8244	0.0245	0.0098	0.0186	81.83	32.5896	0.94	99.36	303.3	2.8	0.0169
1430	50.0326	0.0600	0.0000	0.0237	65.57	32.3039	0.26	100.00	300.8	3.1	0

W = 27.26 mg, J = 0.005617; Total age = 302.0 Ma; F = $^{40}Ar^*/^{39}Ar$, is the ratio of radiogenic Argon 40 and Argon 39.

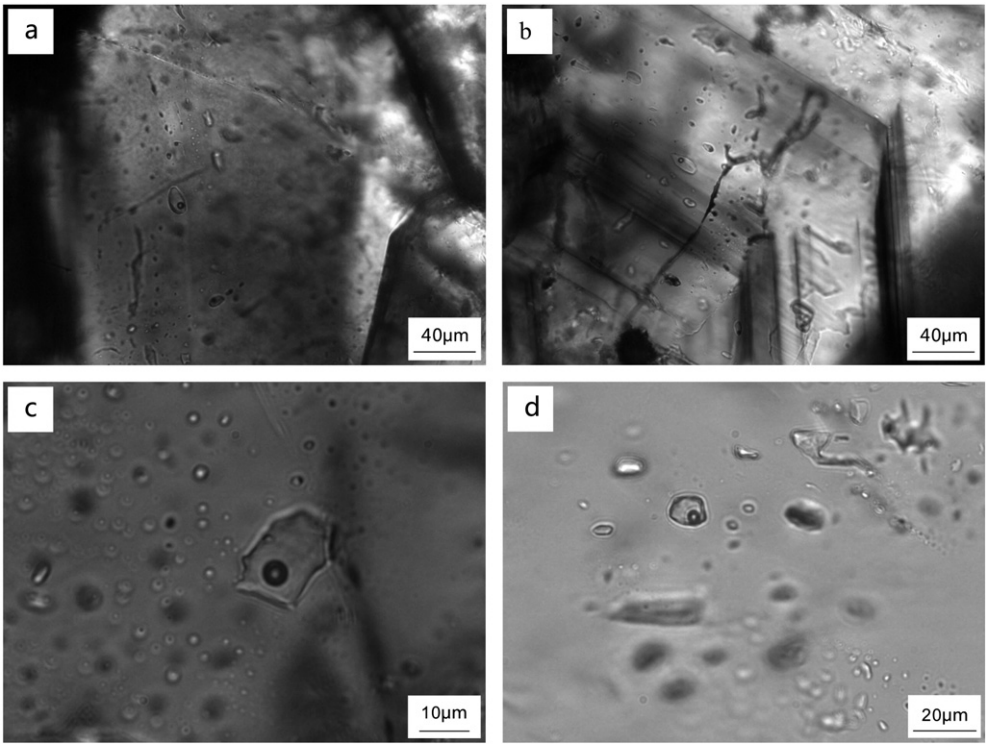

Fig. 7. Transmitted light images showing fluid inclusions of fluorite veins formed in different stages. (a) Fluid inclusions in dark-purple fluorite; (b) Fluid inclusions in zoned purple fluorite; (c) Fluid inclusions in white fluorite; and (d) Fluid inclusions in purple fluorite.

monitors are given in Table 2. The detailed analytical technique was described by Chen et al. (2002).

4.3. Analysis of fluid inclusions

Fluid inclusions obtained from fluorite were used for microthermometry analysis. They were analyzed on a Linkam THMSG600 heating-freezing stage at the Institute of Mineral Resources, Chinese Academy of Geological Sciences. The microthermometry stage was calibrated using synthetic fluid inclusions. The uncertainties of measurements are ±0.1 °C for freezing and ±2 °C for heating. Salinities of fluid inclusions were calculated from the final melting point of ice for two-phase fluid inclusions using the equations of Bodnar et al. (1985) and Bodnar (1995).

4.4. Trace element analysis of fluorite

Fluorite samples were dissolved in a closed dissolver with hydrofluoric acid and nitric acid and evaporated on an electric hot plate to thoroughly remove the hydrofluoric acid. Then, the samples were hermetically dissolved with nitric acid, diluted, and directly measured with ICP-MS using an external standard method. The analyses were performed at the Analytical Laboratory of China National Nuclear Corporation of Beijing Institute of Uranium Geology. The REE tetrad effects for fluorite samples of different stages were calculated according to the method given in Monecke et al. (2007, 2011).

Table 3
Microthermometry analyzing results of fluid inclusions obtained in fluorite from the Baiyanghe deposit, China.

Sample	Th (°C)	Tm (CO_2) (°C)	Salinity (wt.% NaCl)	Number of FI studied
Purple fluorite	130–150	−5.9–6.7	19.7–4.7	79
White fluorite	120–125	0.1–6.1	15.4–7.3	33

4.5. H and O isotopic analysis of muscovite

Oxygen was liberated from muscovite by reacting the samples with BrF_5 (Clayton and Mayeda, 1963; Clayton et al., 1972) and converting to CO_2 on a platinum-coated carbon rod. The $\delta^{18}O$ determinations were performed on a MAT-253 mass spectrometer. Reproducibility for isotopically homogeneous pure muscovite was about ±0.1‰ (1σ). Hydrogen isotope ratios of muscovite and illite were measured by mechanical crushing at 15 mm, following the method described by Simon (2001). The released water was trapped, reduced to H_2 with zinc at 450 °C according to a procedure adapted from Coleman et al. (1982), and then analyzed with a MAT-253 mass spectrometer. Analyses of standard water samples indicate a precision of ±3‰ (1σ) for δD.

4.6. Pb isotopic analysis

Lead column chromatography was performed in a low Pb contamination chemistry laboratory at the Analytical Laboratory of China National Nuclear Corporation of Beijing Institute of Uranium Geology. Whole-rock and ore powders were digested in HF, HCl, and HBr. All samples were eluted using combined HBr–HCl chemistry on Dowex AG-X8 anion exchange resin. Lead was loaded onto a Re ribbon using a silica gel–H_3PO_4 mixture and then analyzed on an ISOPROBE-T thermal ionization mass spectrometer by simultaneous collection of Pb isotope masses. Measured isotopic ratios were corrected for a mass fractionation of 0.11% per atomic mass unit, determined by replicating

Table 4
Stable isotope data of hydrothermal muscovite from the Baiyanghe deposit, northwest China.

Sample	Mineral	$\delta^{18}O_{mineral}$	$\delta^{18}D_{mineral}$	$\delta^{18}O_{H_2O}$	$\delta^{18}D_{H_2O}$	T (°C)
BY12-29	Muscovite	7.8	−124.6	−3.2	−99.6	130
BY12-58	Muscovite	7.2	−135.7	−3.8	−110.7	130
ZK6026-7	Muscovite	7.2	−81.0	−3.8	−56.0	130
ZK13101-3	Muscovite	6.3	−115.6	−4.7	−90.6	130

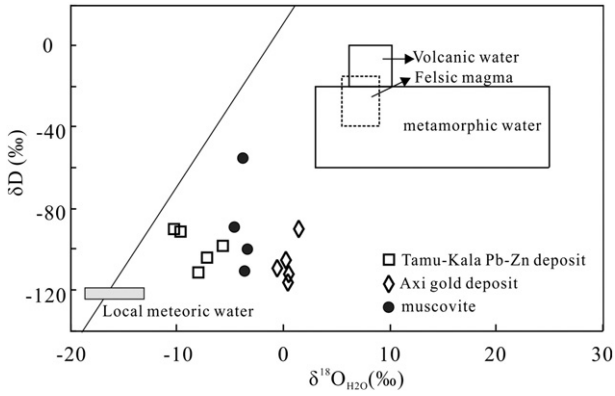

Fig. 8. δD vs. $\delta^{18}O_{H_2O}$ diagram of fluids from muscovite + bertrandite fluorite veins. The fields represent simplified metamorphic fluids (Taylor, 1974), mantle-derived fluids (Sheppard, 1981; Taylor, 1974), volcanic vapors, felsic magma, magmatic water (Hedenquist and Lowenstern, 1994), and local meteoric water (Wang et al., 2002).

the measurement on a Pb standard NBS-981. The total uncertainty is <0.1%. Total blanks contain less than 1 ng of Pb.

Lead, uranium, and thorium concentrations measured on an ELEMENT XR ICP-MS at the Analytical Laboratory of China National Nuclear Corporation of Beijing Institute of Uranium Geology were used to correct for present-day Pb isotope composition for time-integrated growth. The analytical uncertainty of the concentrations is <10%.

5. Analytical results

5.1. Muscovite Ar–Ar dating

The ages and 2σ uncertainties are plotted against the cumulative released ^{39}Ar fraction to establish an age spectra (Fig. 6, Table 2). The Ar isotope ratios are presented on isotope correlation plots using Isoplot of Ludwig (2001). The ^{40}Ar–^{39}Ar data incorporate the apparent age spectra and the atmospheric argon and Ca:K ratios from each heating. The muscovite from sample BH-1 yields a plateau age of 303.0 ± 1.6 Ma, calculated from steps 3–15, representing 98.7% of the total argon release (Fig. 6a). The isochron age of 300.8 ± 2.9 Ma (MSWD = 3.4, initial $^{40}Ar/^{36}Ar = 305$) is concordant with the plateau age (Fig. 6b).

5.2. Fluid inclusions

Assemblages of fluid inclusions (Goldstein and Reynolds, 1994) within fluorite were identified based on petrographic observations

Table 5
Trace elemental compositions of fluorite from the Baiyanghe deposit, northwest China.

Sample	ZK46-1	ZK46-2	ZK60-1	ZK13-1	ZK13-5	ZK13-6	ZK13-3	BY12-58	ZK1432-1	ZK4612-3
	White	White	Green	Green	Green	Light purple	Purple zoned	Dark-purple	Dark-purple	Dark-purple
ppm										
Li	0.896	0.698	1.47	1.25	0.673	5.61	1.45	42.8	1.95	14.6
Be	0.152	0.144	0.26	0.66	0.448	0.53	2	10.2	0.612	233
Sc	1.01	1.05	1.25	0.964	2.27	1.11	3.11	174	1.03	7.69
V	0.166	0.124	0.199	0.055	0.089	0.088	0.034	16.1	0.357	4.52
Cr	1.72	0.305	0.623	0.404	1.31	2.31	0.422	0.567	0.427	2.33
Co	9.83	10.3	10.4	8.04	11	10.6	9	13.3	9.4	7.89
Ni	0.752	0.061	0.053	0.255	0.48	0.999	0.058	1.02	0.143	2.28
Cu	2.02	0.009	<0.002	0.339	2.09	0.153	0.159	2.4	0.461	2.15
Zn	7.66	3.24	3.75	5.34	1.71	2.65	2.15	65.5	2.01	63.2
Ga	0.251	0.185	0.738	0.435	0.387	0.319	0.371	2.8	0.297	5.22
Rb	0.219	0.13	0.427	0.242	0.124	0.419	0.418	23.3	0.741	36.2
Sr	250	262	174	964	1121	945	1906	339	214	3075
Y	102	43	102	433	387	159	312	159	52.1	189
Nb	0.079	0.04	0.123	0.077	0.191	0.041	0.153	3.13	0.654	12.9
Mo	0.214	0.111	0.159	0.182	0.444	0.448	0.047	9.18	0.196	3.44
Cd	0.116	0.027	0.071	0.042	0.028	0.018	0.014	0.091	0.008	0.401
Sb	0.351	0.161	0.248	0.234	0.098	0.583	0.313	2.37	0.313	0.586
Cs	0.154	0.127	0.324	0.294	0.011	0.516	0.387	9.71	0.482	4.19
Ba	0.994	0.814	2.02	2.68	2.36	2.98	7.82	35.9	1.38	28.8
La	9.59	7.55	13.3	10.9	10.1	7.7	9.19	35.7	7.53	13.9
Ce	19.4	14.5	39	26.7	24.8	19.5	31.3	114	15.8	30
Pr	2.46	1.82	7.57	4.27	4	2.9	4.44	15.6	1.55	3.33
Nd	11.7	8.42	44.2	25.3	23.6	15.7	16.4	53.8	4.6	11.4
Sm	4.43	2.85	20.3	18.8	17.2	8.75	9.55	15.1	1.28	5.6
Eu	5.35	2.82	13.5	1.46	1.3	0.676	0.537	2.67	0.188	0.564
Gd	4.83	3.01	16.9	32.1	28.5	12.3	10.2	13	1.39	7.32
Tb	1.17	0.711	3.29	10.5	9.25	3.95	4.29	3.04	0.353	2.21
Dy	9.15	5.39	17.3	77.7	70.6	30	47.9	23.9	3.28	19.8
Ho	1.94	1.13	2.4	12.6	11.3	4.93	11.6	5.6	0.927	4.72
Er	5.1	3.03	4.59	24.3	22.2	10.3	41.1	19.6	3.52	15.4
Tm	0.844	0.508	0.481	3.08	2.86	1.44	9.98	4.67	0.911	3.39
Yb	5.03	3.05	2.95	15.1	14.2	7.43	73	35	7.4	23.6
Lu	0.74	0.467	0.381	1.92	1.84	0.938	9.35	5.54	1.32	3.59
Ta	0.109	0.067	0.084	0.285	0.403	0.134	0.269	0.275	0.096	1.23
W	0.46	0.325	0.278	0.67	0.721	0.335	1.02	2.19	0.281	1.01
Re	0.018	0.01	0.009	0.056	0.063	0.027	0.16	0.085	0.016	0.06
Tl	0.002	<0.002	<0.002	<0.002	0.008	0.003	<0.002	0.115	0.003	0.12
Pb	3.23	6.32	5.32	1.07	1.82	1.05	1.55	13.8	3.61	163
Bi	0.01	0.008	0.007	0.005	0.004	0.014	0.01	139	0.069	0.324
Th	0.027	0.018	0.126	5.88	6.77	1.3	13.7	136	1	17.6
U	0.032	0.017	0.213	0.086	0.069	0.089	0.359	5.73	0.332	2.51
Zr	0.275	0.279	11.3	0.623	7.41	1.18	3.12	0.702	4.12	55.4
Hf	0.321	0.191	0.796	2.44	2.77	0.962	1.61	0.795	0.309	3.22

Table 6
Sizes of tetrads in the rare earth element patterns, from the Baiyanghe deposit, northwest China.

Sample	ZK46-1*	ZK46-2*	ZK60-1#	ZK13-1#	ZK13-5#	ZK13-3**	ZK13-6®	BY12-58©	ZK1432-1©	ZK4612-3©
LaN/YbN	1.32	1.71	3.12	0.50	0.49	0.09	0.72	0.71	0.70	0.41
Yn/DyN	1.73	11.17	0.39	0.20	0.95	1.01	0.82	1.04	2.47	1.49
Eu/Eu*	3.51	2.92	2.21	0.18	0.18	0.17	0.20	0.58	0.43	0.27
La1/3	3.44	3.18	3.84	3.59	3.50	3.40	3.20	5.34	3.18	3.90
La2/3	11.86	10.11	14.75	12.92	12.28	11.53	10.25	28.50	10.10	15.19
Nd1/3	2.96	2.65	4.61	3.82	3.74	3.31	3.26	4.92	2.17	2.93
Nd2/3	8.75	7.02	21.21	14.62	13.96	10.95	10.64	24.18	4.69	8.60
T′	0.01	0.01	0.00	0.01	0.01	0.13	0.00	0.12	0.04	0.01
T″	0.01	0.01	0.00	0.01	0.01	0.12	0.00	0.13	0.03	0.01
T1	0.08	0.09	0.05	0.10	0.09	0.35	0.04	0.35	0.18	0.12
Gd1/3	2.91	2.48	4.41	5.47	5.25	3.73	3.97	4.04	1.92	3.34
Gd2/3	8.45	6.17	19.48	29.87	27.60	13.91	15.76	16.35	3.68	11.15
Ho1/3	3.27	2.73	3.51	6.10	5.88	5.93	4.46	4.65	2.55	4.39
Ho2/3	10.68	7.45	12.31	37.17	34.57	35.18	19.88	21.65	6.53	19.32
T′	0.03	0.03	0.11	0.35	0.33	0.19	0.30	0.01	0.00	0.06
T″	0.05	0.04	0.10	0.33	0.36	0.25	0.32	0.02	0.01	0.07
T3	0.19	0.18	0.32	0.58	0.59	0.47	0.56	0.11	0.06	0.25
Er1/3	3.18	2.67	3.07	5.35	5.19	6.37	4.02	4.98	2.81	4.59
Er2/3	10.10	7.14	9.41	28.60	26.92	40.60	16.14	24.78	7.89	21.10
Lu1/3	3.12	2.68	2.50	4.29	4.23	7.27	3.38	6.11	3.79	5.29
Lu2/3	9.75	7.17	6.26	18.41	17.90	52.90	11.42	37.32	14.34	27.95
T′	0.01	0.01	0.02	0.00	0.00	0.16	0.01	0.08	0.07	0.07
T″	0.00	0.00	0.00	0.00	0.00	0.11	0.00	0.03	0.02	0.02
T4	0.07	0.07	0.12	0.05	0.05	0.37	0.06	0.22	0.21	0.20

The data with *, #, **, ®, and © indicate the color of white, green, zoned purple, light purple, and dark-purple, respectively.

and microthermometry. Single and isolated fluid inclusions were avoided (Roedder, 1984). Different types of fluid inclusions were distinguished according to the phases present at 25 °C and their volume proportions. Fluid inclusions were classified as primary, secondary, or pseudosecondary according to the definitions of Roedder (1984) and Shepherd et al. (1985). Two major types were recognized within the primary fluid inclusions based on the phases present at room temperature and the homogenization behavior (Cline and Vanko, 1995), which are (1) Type-1: CO_2-bearing liquid-rich fluid inclusions, and (2) Type-2: three-phase (V–L–L) of liquid-H_2O with vapor–liquid CO_2 fluid inclusions (Fig. 7; Table 3). However, a method to calculate salinities of CO_2-bearing H_2O inclusions does not exist. Using the assumption that the liquid CO_2 content in the CO_2-bearing liquid-rich inclusions is infinitely close to zero, the salinities of such inclusions can be calculated.

Fluid inclusions in the dark-purple fluorite are dominated by Type-1 fluid inclusions with lesser Type-2 fluid inclusions. The inclusions are round and/or oval in shape, with sizes up to 20 μm (5–20 vol.%). Measurements of Type-1 fluid inclusions within the dark-purple fluorite suggest that this type of fluorite was produced from homogeneous, low-temperature hydrothermal fluids. Homogenization temperatures (Th) range from 120 °C to 125 °C, with salinity ranging from 7.3 to 15.0% NaCl eqv. Measurements of Type-2 three-phase (V–L–L) fluid inclusions in the dark-purple fluorite show CO_2 clathrate melting temperatures ranging from −5.9 °C to 6.6 °C.

Fluid inclusions in the white fluorite are also dominated by Type-1 fluid inclusions with lesser Type-2 fluid inclusions. They are round and/or oval in shape, with sizes up to 20 μm (10 vol.%). Measurements of Type-1 fluid inclusions in the white fluorite suggest that this type of fluorite was also precipitated from homogeneous, low-temperature hydrothermal fluids. Homogenization temperatures (Th) range from 120 °C to 125 °C, with salinity ranging from 7.3% to 15.4% NaCl eqv. Measurements of Type-2 fluid inclusions in the early fluorite show CO_2 clathrate melting temperatures ranging from 0.1 °C to 6.1 °C. Several fluid inclusions in the dark-purple and white fluorite have CO_2 clathrate melting temperatures higher than 10 °C, suggesting the existence of other gaseous components such as CH_4 within the fluid inclusions (Collins, 1979).

5.3. O and H isotopes of muscovite

The $\delta^{18}O$ and δD values of the muscovite samples collected from dark-purple, Be–U–Mo-bearing fluorite veins range from 7.2 to 7.8‰, and −135.7 to −124.6‰, respectively. The $\delta^{18}O$ and δD values of the muscovite collected from the altered granite porphyry range from 6.3 to 7.2‰ and −115.6 to −81.0‰, respectively (Table 4). The $\delta^{18}O$ and δD values of the hydrothermal fluids that are responsible for formation of muscovite are calculated (Sheppard and Gilg, 1996; Zheng, 1993) at a temperature of 130 °C, which is a median temperature based on analysis of fluid inclusions. As a result, they show −3.2 to −3.8‰ and −4.7 to −3.8‰ for $\delta^{18}O$, and −110.6 to −99.6‰ and −90.6 to −56.0‰ for δD (Fig. 8).

5.4. Trace element concentrations of fluorite

The trace element concentrations of fluorite of different stages are listed in Table 5. The fluorite generated in different stages shows varied concentrations of Nb, Sr, Co, Li, Zn, Rb, U, Be, Mo, and ΣREE. The earliest dark-purple fluorite contains the highest concentration of U, Be, and Mo, whereas the younger fluorite has either higher Be or higher Mo concentrations.

The REE patterns of the earliest dark-purple fluorite is characterized by variable ΣREE concentrations (50.1×10^{-6} to 347.2×10^{-6}) and lower Tb/La ratios (0.05–0.51), with negative δEu anomalies and positive δCe anomalies. The younger green fluorite has higher but also variable REE concentrations (186.2×10^{-6} to 264.7×10^{-6}) and Tb/La ratios (0.18–2.23), with negative δCe anomalies (0.95–0.96). The pure green fluorite has positive δEu anomalies (2.23). The intergrowth within the purple fluorite has negative δEu anomalies (0.18). The youngest white fluorite exhibits low REE abundances, flat REE patterns, lower Tb/La ratios (0.09–0.12), negative δCe anomalies (0.96–0.98), and pronounced positive δEu anomalies (2.9–3.5).

The REE patterns exhibit either convex or concave tetrads (Table 6; Fig. 9). The sizes of the third convex or concave tetrads are significant in the dark-purple fluorite, whereas the first and fourth tetrads are more subtle but still significant in most cases.

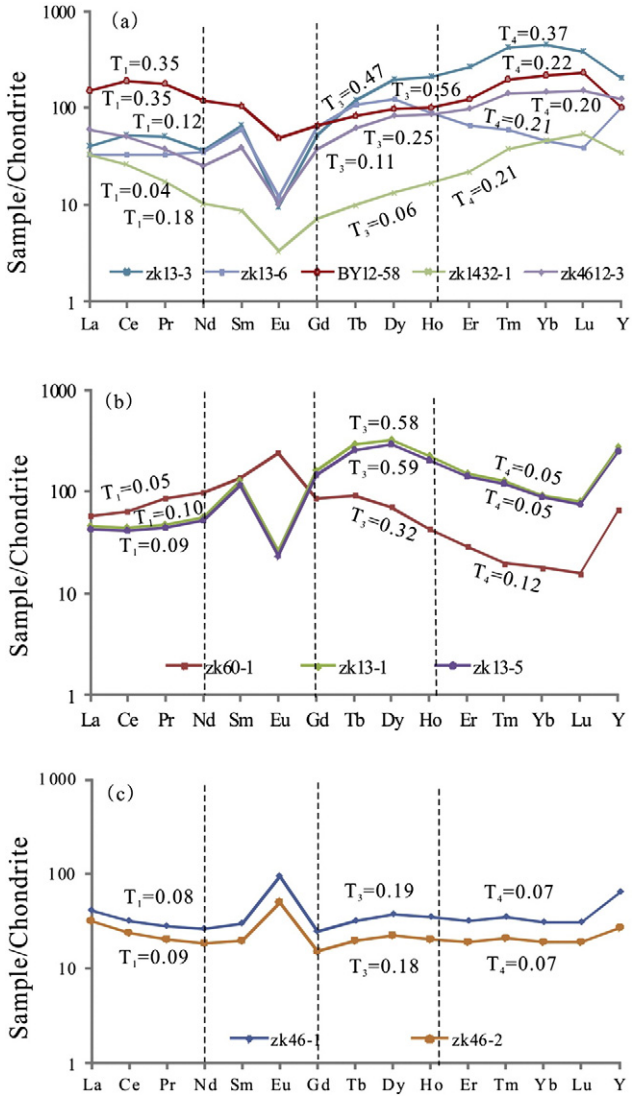

Fig. 9. Normalized rare earth element (REE) patterns of selected fluorite samples. (a) REE patterns for fluorite in dark-purple, zoned purple, and purple colors. (b) REE patterns of green fluorite. (c) REE pattern of white fluorite. Ti values represent the size of individual tetrads.

5.5. Pb isotopes

Pb isotope compositions of the 13 whole rock samples and 3 ore samples are listed in Table 7. The $^{206}Pb/^{204}Pb$, $^{207}Pb/^{204}Pb$, and $^{208}Pb/^{204}Pb$ values for the granite porphyry samples range from 18.731 to 19.300, 15.523 to 15.586, and 38.095 to 38.961, respectively. For the granite samples, the values range from 18.184 to 18.691, 15.498 to 15.528, and 37.945 to 38.467, respectively. The $^{206}Pb/^{204}Pb$, $^{207}Pb/^{204}Pb$, and $^{208}Pb/^{204}Pb$ values for the Devonian volcanic rocks range from 18.108 to 18.710, 15.496 to 15.547, and 37.830 to 38.084, respectively. The diabase has relatively lower Pb isotope compositions ($^{206}Pb/^{204}Pb$ = 17.976–18.268, $^{207}Pb/^{204}Pb$ = 15.492–15.525, and $^{208}Pb/^{207}Pb$ = 37.764–38.006). Time-corrected Pb isotope composition values of the mineralized samples are between the diabase and the granite porphyry samples (Fig. 10).

6. Discussion

6.1. The age of Be–U–Mo mineralization

There is debate regarding the age of Be–U mineralization at the Baiyanghe deposit because no suitable minerals for dating were available. Researchers have tried to use the emplaced ages of the Yangzhuang granite porphyry and diabase dikes to indirectly represent the age of mineralization, such as the granite porphyry whole rock Rb–Sr age of 293 ± 15 Ma (Ma et al., 2010), the zircon LA–ICP-MS U–Pb ages of 309.2 Ma (Ma et al., 2010) and 313 ± 2.3 Ma (Zhang et al., 2014), and the diorite dike whole rock Rb–Sr age of 298 ± 18 Ma. Because the whole rock Rb–Sr ages have a larger error and the zircon grains have higher uranium concentrations, the resulting ^{206}Pb–^{235}U ages may be indefinite. These age data cannot be used to constrain the age of Be–U mineralization well. Ma et al. (2010) dated the seven pitchblende U–Pb ages, and obtained ages of 224 ± 3.1 Ma, 237.8 ± 3.3 Ma, 197.8 ± 2.8 Ma, 97.8 ± 1.4 Ma and 30.0 ± 0.4 Ma. However, these data do not provide a better interpretation of the age of U–Be mineralization at the Baiyanghe deposit because this group of pitchblende ages has large scatter among the data.

The muscovite sample we collected occurred within the muscovite–fluorite veins. The fluorite is dark-purple and is associated with Be mineralization (Fig. 5a). The sample BH-1 muscovite has a plateau age of 303.0 ± 1.6 Ma, representing 98.7% of the total argon release. This indicates that there was no late hydrothermal activity overprint. Therefore, the new muscovite Ar–Ar age reports in this paper provide a better constraint on the timing of the U–Be mineralization for the Baiyanghe deposit. The Be–U–Mo mineralization at the Baiyanghe deposit occurred in the Late Carboniferous.

6.2. Relationship between fluorite and Be–U–Mo mineralization

Gangue minerals offer important information about the conditions and processes of mineralization of hydrothermal ore deposits. Generally, it is reasonable to assume that the hydrothermal solutions that produced gangue minerals were nearly in equilibrium with ore minerals at the time of mineralization (Barnes, 1997). Fluorite is an important

Table 7
Pb isotopic data of volcanic rocks, granite, and ores from the Baiyanghe deposit, northwest China.

Sample	Rock type	Pb (ppm)	Th (ppm)	U (ppm)	$^{206}Pb/^{204}Pb$	2σ	$^{207}Pb/^{204}Pb$	2σ	$^{208}Pb/^{204}Pb$	2σ
BYP1-12	Mo ore	92.2	30.4	6.5	18.354	0.002	15.523	0.002	38.059	0.004
BYP1-20	Granite porphyry	31.6	20.8	5.1	19.300	0.004	15.586	0.003	38.961	0.008
7702-1	Granite porphyry	29.2	24.6	3.5	18.731	0.001	15.547	0.001	38.587	0.003
BYP1-32	Granite porphyry	43.3	9.5	4.1	18.184	0.002	15.498	0.002	37.945	0.004
BY10-11	Diabase	7.2	2.2	1.0	18.268	0.002	15.502	0.001	38.006	0.004
BY10-04	Diabase	7.1	2.1	0.9	18.248	0.001	15.525	0.001	37.880	0.003
BYP2-14	Diorite	19.6	5.8	3.3	18.319	0.001	15.518	0.001	38.079	0.003
BYP1-09	Basalt	15.0	1.1	0.7	18.108	0.001	15.506	0.001	37.830	0.003
BYP1-01	Rhyolite	72.4	7.4	3.1	18.166	0.001	15.547	0.001	37.990	0.003
BYP1-02	Rhyolite	33.5	9.4	2.4	18.171	0.001	15.506	0.001	38.013	0.002
BYP1-05	Be ore	41.4	10.2	3.0	18.161	0.002	15.496	0.002	37.955	0.004
BYP1-07	Diabase	132.0	0.84	0.41	17.976	0.002	15.492	0.001	37.764	0.003
ZK8012	Be ore	22.2	27.2	6.0	19.365	0.001	15.563	0.001	39.111	0.003

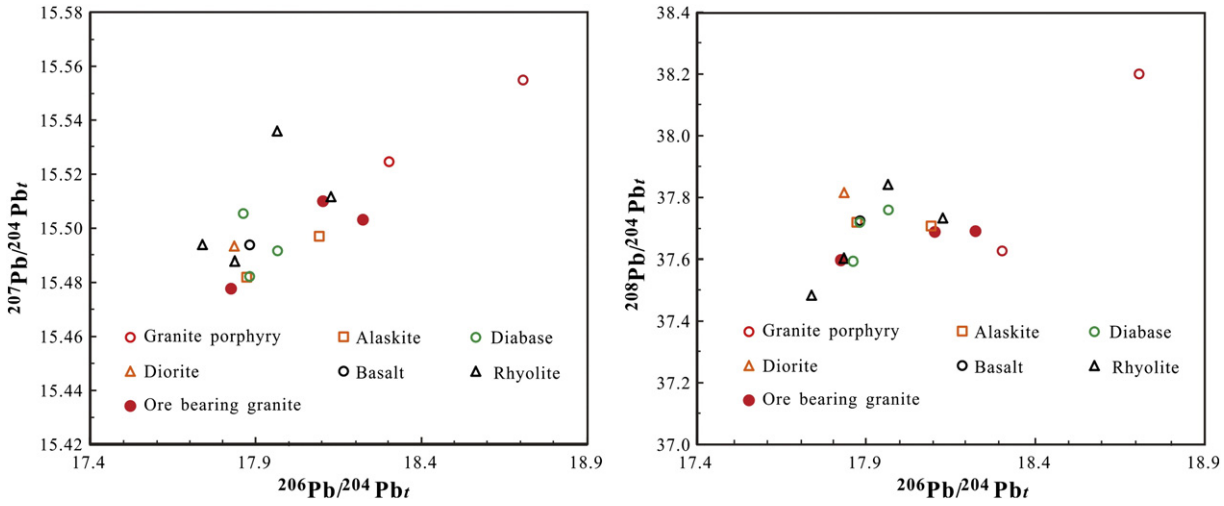

Fig. 10. Uranogenic (a) and thorogenic (b) diagrams for comparison of time-corrected Pb isotopic compositions of Yangzhuang granite porphyry, diabase, diorite, granite, and Late Devonian rhyolite, basalt, and tuff.

gangue mineral in Be–U deposits. Its geochemistry allows direct reconstruction of the chemistry of the hydrothermal fluids sourced from the magma–fluid system. Fluorite REE patterns and the size of individual tetrads are also helpful for characterizing the evolution of hydrothermal fluids (Constantopoulos, 1988; Graupner et al., 1999; Jebrak et al., 1985; Monecke et al., 2002; Möller and Dulski, 1999; Morozov et al., 1996; Trinkler et al., 2005).

Based on field observations, the bertrandite in the Baiyanghe deposit is intergrown with dark-purple fluorite and muscovite (Fig. 5a), indicating that the Be mineralization is associated with the dark-purple fluorite. The higher Mo, U, and Be concentrations in the dark-purple fluorite also suggest a close relationship with Mo, U, and Be mineralization. Green fluorite intergrowths within the light purple fluorite show Be, Mo, and U anomalies, whereas the pure green fluorite has no Be, Mo, and U anomalies. This again indicates a close relationship of the purple fluorite with the mineralization. The white fluorite shows no Be, Mo, and U anomalies.

The REE patterns of fluorite of different colors show neither concave nor convex tetrads, and have neither positive nor negative δ Eu anomalies. Fluorite with higher U, Be, and Mo concentrations also has higher T sizes (>0.1) of sub-tetrads (e.g., sample BY12-58), whereas fluorite with lower U, Be, and Mo concentrations has lower T sizes of sub-tetrads (e.g., sample ZK1432-1). The green and white fluorites that are not closely associated with mineralization have lower T sizes of the first and fourth tetrads (<0.01), although their third tetrad has higher T sizes (0.18–0.19).

The origin of REE tetrads in evolved granite and associated hydrothermal systems has been a topic under considerable debate (Bau and Dulski, 1999; Irber, 1999; Monecke et al., 2002; Yurimoto et al., 1990). Early researchers suggested that convex tetrads in evolved granitic rocks were caused by fractional crystallization of accessory phases from melts (Yurimoto et al., 1990). Irber (1999) proposed that the convex tetrads in granite REE patterns were formed from open-system melt crystallization, whereas the complementary concave tetrads were developed in coexisting external fluids or exsolved magmatic–hydrothermal fluids that subsequently migrated away from magmatic intrusions. Minerals from hydrothermal veins associated with evolved granite intrusions commonly exhibit convex tetrads (Monecke et al., 2002). Zhao et al. (2010) proposed that the composite M- and W-type REE tetrad effect of the Shuiquangou alkaline complex in northern China resulted from co-existing melt and aqueous phases of high temperature, high salinity fluids. In short, these studies indicate that the origin of REE tetrads in minerals and granitic rocks is a complicated issue.

The characteristics of fluid inclusions in fluorite of different colors suggest that low temperature hydrothermal fluids were involved in the Be–U–Mo mineralization at the Baiyanghe deposit. Fluid immiscibility has not been found in the study. Complementary tetrads are not observed in fluorite of different colors. It is suggested that significant fluid mixing could be responsible for Be–U–Mo mineralization and that precipitation of fluorite occurred from the original saline aqueous fluids.

6.3. Sources of U, Be, and Mo

The Yangzhuang granite porphyry is considered to be a possible source for the U, Be, and Mo metals. The major elemental analysis shows that the porphyry has an A_1-type affinity (Eby, 1992; Whalen et al., 1987), with high contents of SiO_2 (75.2–78.3 wt.%), $Na_2O + K_2O$ (7.83–9.03 wt.%), and Al_2O_3 (12.3–13.1 wt.%); low contents of CaO (0.29–1.00 wt.%); and relatively high Fe/Mg ratios (Mao et al., 2014). In its primitive mantle-normalized spider diagram, the porphyry shows significant enrichment of Th, U, Nb, and Ta and depletion of Ba, Sr, Eu, P, and Ti. The porphyry has high contents of F, Ga, Sn, Y, and rare earth elements. Both Nb and Ta contents are nearly 10 times higher than the coeval granite of A_2-type affinity in the region (Geng et al., 2009, 2011; Mao et al., 2014; Su and Tang, 2005; Tang et al., 2010). These A2-type granites have no Be–U mineralization. U and Be concentrations in the Yangzhuang granite porphyry are 17.2×10^{-6} and 13.2×10^{-6}, respectively, which are higher than in average granite, suggesting that the porphyry might be the source of the ore metals, e.g., U, Be, and Mo, in the deposit.

Fig. 11 demonstrates the correlation of Nb–U, Nb–Be, and Nb–Mo, which suggests that Be, U, and Mo in the Baiyanghe deposit might be sourced from the Yangzhuang granite porphyry.

Time-corrected Pb isotopic compositions of the Be–U ore samples plot in between the granite porphyry and the diabase (Fig. 10). The diabase has lower $^{206}Pb/^{204}Pb$ and $^{207}Pb/^{204}Pb$ ratios, whereas the granite porphyry shows higher $^{206}Pb/^{204}Pb$ and $^{207}Pb/^{204}Pb$ ratios. It is suggested that Pb in the Be–U ore may be derived from both diabase and granite. As observed in the deposit, the diabase is closely spatially associated with the Be–U–Mo mineralization.

6.4. Fluid mixing and Be–U–Mo mineralization

Analyses of the fluid inclusions from the Be–U–Mo-bearing fluorite give homogenization temperatures ranging from 120 °C to 150 °C. No pressure corrections are required for homogenization temperatures

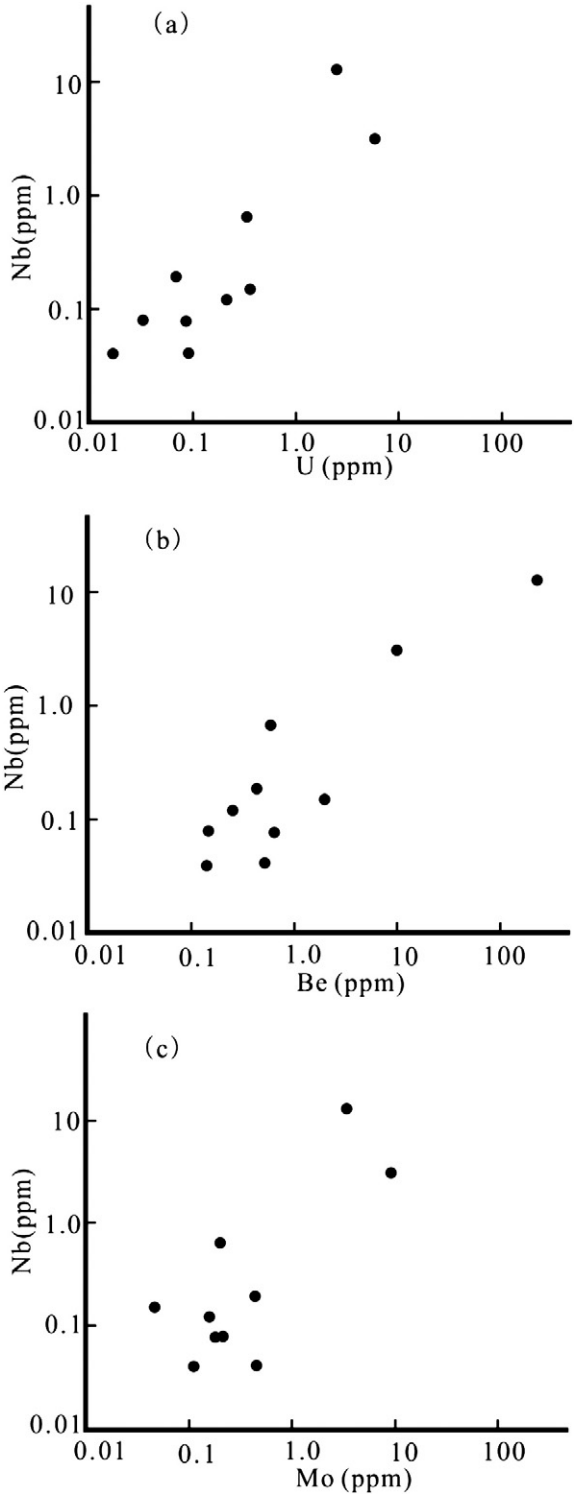

Fig. 11. Correlation between Nb and U, between Nb and Mo, and between Nb and Be in fluorite in the Baiyanghe deposit.

because most of the fluid inclusions in fluorite are dominated by liquid-rich inclusions (Chi and Lai, 2009). The trapped temperature for fluid inclusions in fluorite also ranges from 120 °C to 150 °C. This result indicates that the Baiyanghe U–Be–Mo deposit is an epithermal deposit.

The fluid inclusions in fluorite are dominated by liquid-rich inclusions, but most of these fluid inclusions contain less CO_2. CO_2 clathrate melting temperatures in the Type-2 fluid inclusions also suggest that other gas compositions can be contained within the fluid inclusion. The measured salinities in the fluid inclusions range from 4.7% NaCl eqv. to 19.7% NaCl eqv. The homogenization temperatures vary slightly, but the average salinities change dramatically. Therefore, some other source of high salinity fluid is needed in addition to meteoric water.

Taking the geologic setting into account, magmatic water could be an important source of ore forming fluids. Meteoric and magmatic waters could mix to produce ore-forming fluids with salinity ranging from 4.7% NaCl eqv. to 19.7% NaCl eqv. The $\delta^{18}O$ and δD values for the hydrothermal fluids that are responsible for the mineralization range from −4.7 to −3.2‰, and from −110.6 to 56.0‰, respectively. These data plot between magmatic water and local meteoric water (Fig. 8), similar to the hydrothermal fluids in the Axi gold deposit (Zhai et al., 2007) and the Talan–Gulangu Pb–Zn deposit (Wang et al., 2002) in northwest China. This result suggests that the hydrothermal fluids originated from mixing between magmatic and meteoric water.

Under hydrothermal conditions, Eu primarily exists as a divalent cation. The model of Haas et al. (1995) demonstrated that Eu^{2+} strongly associates with Cl^- to form $EuCl^{3-}$ and $EuCl_4^{2-}$. In such hydrothermal solutions, REEs could transport as REE–Cl complexes, resulting in the development of a positive δEu anomaly. However, the model also predicted that complexation of REE and F could result in a negative δEu anomaly in hydrothermal solutions. In the case of the Baiyanghe deposit, the dark-purple fluorite of the earliest-stage shows a negative δEu anomaly, indicating REE–F complexation within hydrothermal solutions. In contrast, the green and white fluorite that formed in later stages show positive δEu anomalies, indicating a REE–Cl complexation.

The geochemistry of uranium is mainly governed by its oxidation state. Generally, U is highly mobile as the hexavalent uranyl ion (UO_2^{2+}) under oxidizing conditions. It may form more than 40 complexes with hydroxyl, carbonate, sulfate, chloride, phosphate, fluoride, and silicate anions (Langmuir, 1978). Uranyl-carbonates predominate at high pH, low temperature, and intermediate to high fO_2. Phosphates predominate at neutral pH. Sulfates and chlorides are important at acidic conditions. In reduced conditions, U^{4+} solubility is extremely low and similar to that of Th. High U^{4+} and Th solubility is limited to high temperatures and is mainly controlled by fluoride complexes. Precipitation of U in most deposits is related to a decrease in fO_2, generally resulting from the interaction of oxidized U-bearing fluids with carbonaceous matter under various states, from anaerobic bacterial activity to graphite. As for beryllium, the mixed fluoride–hydroxide complexes ($BeOHF(aq)$, $Be(OH)_2F^-$) have very restricted fields of predominance and are hence relatively unimportant in the hydrothermal solutions (Wood, 1992). Carbonate complexes ($BeCO_3(aq)$, $Be(CO_3)_2^{2-}$) also contribute negligibly to the solubility of these minerals over the geologically reasonable pH range at 25°–300 °C and free carbonate concentrations (Wood, 1992). It is therefore likely that the Be at the Baiyanghe deposits acted in the form of fluoride complexes in hydrothermal fluids at a temperature between 100° and 200 °C. Mo is dominantly transported as hydroxyl complexes, and high concentrations of Cl may destabilize these complexes and inhibit the transport of these elements (Keppler and Wyllie, 1991). Thus, the hydrothermal fluids responsible for the Be–U–Mo mineralization were CO_2–CH_4–F-rich fluids. However, at later stages, the hydrothermal fluids were predominately CO_2–CH_4–Cl-rich.

Oxidizing saline fluids derived from the diabase could percolate throughout the granite porphyry to remove Be, U, and Mo metals and other trace metals. These metal-rich fluids may then have descended along fractures within the granite porphyry and its contact zones in the Late Devonian tuff. Upon mixing with locally reduced CH_4-rich fluids, which ascended through the Devonian tuff, Be-, U-, and Mo-bearing minerals and dark-purple fluorite were precipitated. Later, the green and white fluorite was precipitated from the CO_2–Cl-rich fluids. The blue, supergene hydrated Mo oxide (e.g., ilsemannite) was superimposed on primary molybdenite, as observed at some high-grade ores.

7. Conclusions

1. The Baiyanghe Be–U–Mo deposit in Northwestern China is genetically related to the Late Carboniferous Yangzhuang granite porphyry. Three stages of fluorite with different colors have been identified at the deposit, of which the earliest-stage, dark-purple fluorite is more closely associated with the Be–U–Mo mineralization.
2. The muscovite Ar–Ar dating has yielded a plateau age of 303.0 ± 1.6 Ma, which constrains the Be–U–Mo mineralization of the deposit to the Late Carboniferous.
3. The Be–U–Mo-bearing fluorite veins were precipitated from hydrothermal fluids of low temperature (120–150 °C) with salinity ranging from 4.7 to 19.7 wt.% NaCl eqv. Primary fluid inclusions from the earliest, dark-purple fluorite, which was coeval with bertrandite, were homogenized at 130–150 °C and have salinities ranging from 4.7 to 19.7 wt.% NaCl eqv. Based on the trace element concentrations and REE patterns of the fluorite, the style of veining, and the low salinity and low temperature characteristics of the fluid inclusions, it is suggested that Be and U were most likely transported as fluoride complexes and Mo as hydroxyl complexes.
4. Pb isotopic compositions of the ores, as well as O and H isotopic characters of the ore-related muscovite suggest mixing between magmatic and meteoric waters; both contributed to formation of the ore-forming fluids. Ore metals, i.e., Be, U, and Mo, could be leached out from the Yangzhuang granite porphyry and transported in oxidized saline fluids. The saline fluids predominantly flowed downward along fractures and the contact zones between the granite porphyry and its country rock (Devonian tuff). The fluid mixing with a temperature decrease led to reduction of U, Mo, and Be and, hence, precipitation of ore at the Baiyanghe deposit.

Acknowledgments

This study was financially supported by the One Hundred Person Project of the Chinese Academy of Sciences and a grant from the China National Nuclear Corporation (CNNC). We are grateful to two anonymous reviewers and Dr. Franco Pirajno for their constructive reviews and significant help in improving the original manuscript. We are grateful to colleagues Yanlong Li and Jian Zhou from the No. 216 Geological Survey of the CNNC for their assistance during the field seasons.

References

Barnes, H.L., 1997. Geochemistry of Hydrothermal Ore Deposits. Wiley-Interscience, New York, p. 486.
Bau, M., Dulski, P., 1999. Comparing yttrium and rare earths in hydrothermal fluids from the Mid-Atlantic Ridge: implications for Y and REE behaviour during near-vent mixing and for the Y/Ho ratio of Proterozoic seawater. Chem. Geol. 155 (1), 77–90.
Bodnar, R.J., 1995. Fluid-inclusion evidence for a magmatic source for metals in porphyry copper deposits. In: Thompson, J.F.H. (Ed.), Magma, Fluid and Ore Deposit (Mineralogical Association of Canada Short Course Series)vol. 23. Mineralogical Association of Canada, Victoria, British Columbia, pp. 139–152.
Bodnar, R.J., Burnham, C.W., Sterner, S.M., 1985. Synthetic fluid inclusions in nature quartz. III. Determination of phase equilibrium porphyries in the system H_2O–NaCl to 1000 °C and 1500 bars. Geochim. Cosmochim. Acta 49, 1861–1873.
Chen, W., Zhang, Y., Ji, Q., Wang, S.S., Zhang, J.X., 2002. The magmatism and deformation times of the Xidaatan rock series, East Kunlun Mountain. Sci. China (Ser. B) 45, 20–27.
Chen, J.F., Han, B.F., Ji, J.Q., Zhang, L., Xu, Z., He, G.Q., Wang, T., 2010. Zircon U–Pb ages and tectonic implications of Paleozoic plutons in northern West Junggar, North Xinjiang, China. Lithos 115 (1–4), 137–152.
Chi, G.X., Lai, J.Q., 2009. Roles of fluid inclusions in study of mineral deposits. Miner. Depos. 28 (6), 850–855.
Clayton, R.N., Mayeda, T.K., 1963. The use of bromine pentafluoride in the extraction of oxygen from oxides and silicates for isotopic analysis. Geochim. Cosmochim. Acta 27, 43–52.
Clayton, K.N., O'Neil, J.R., Mayeda, T.K., 1972. Oxygen isotope exchange between quartz and water. J. Geophys. Res. 77, 3057–3067.
Cline, J.S., Vanko, D.A., 1995. Magmatically generated saline brines related to molybdenum at Questa, New Mexico, USA. In: Thompson, J.F.H. (Ed.), Magma, Fluid and Ore Deposit (Mineralogical Association of Canada Short Course Series)vol. 23. Mineralogical Association of Canada, Victoria, British Columbia, pp. 153–174.
Coleman, M.L., Shepherd, T.J., Durham, J.J., Rouse, J.E., Moore, G.R., 1982. Reduction of water with zinc for hydrogen isotope analysis. Anal. Chem. 54, 993–995.
Collins, P.L.F., 1979. Gas hydrates in CO_2-bearing fluid inclusions and the use of freezing data for estimation of salinity. Econ. Geol. 74 (6), 1435–1444.
Constantopoulos, J., 1988. Fluid inclusions and rare earth element geochemistry of fluorite from south-central Idaho. Econ. Geol. 83 (3), 626–636.
Dong, L.H., Feng, J., Liu, D.Q., Tang, Y.L., Qu, X., Wang, K.Z., Yang, Z.F., 2010. Research for classification of metallogenic unit of Xinjiang. Xinjiang Geol. 28 (1), 1–15.
Eby, G.N., 1992. Chemical subdivision of the A-type granitoids: petrogenetic and tectonic implications. Geology 20, 641–644.
Fayek, M., Shabaga, B., 2011. The Baiyanghe beryllium deposit, NW China. Intern. Rep. 1–26.
Geng, H.Y., Sun, M., Yuan, C., Xiao, W.J., Xian, W.S., Zhao, G.C., Zhang, L.F., Wong, K., Wu, F.Y., 2009. Geochemical, Sr–Nd and zircon U–Pb–Hf isotopic studies of Late Carboniferous magmatism in the West Junggar, Xinjiang: implications for ridge subduction? Chem. Geol. 266, 364–389.
Geng, H.Y., Sun, M., Yuan, C., Zhao, G.C., Xiao, W.J., 2011. Geochemical and geochronological study of early Carboniferous volcanic rocks from the West Junggar: petrogenesis and tectonic implications. J. Asian Earth Sci. 42, 854–866.
Goldstein, R.H., Reynolds, T.J., 1994. Systematics of fluid inclusions in diagenetic minerals. Soc. Sed. Geol. Short Course 31 (1994, 199 p.).
Graupner, T., Kempe, U., Dombon, E., 1999. Fluid regime and ore formation in the tungsten (–yttrium) deposits of Kyzyltau (Mongolian Altai): evidence for fluid variability in tungsten–tin ore systems. Chem. Geol. 154 (1), 21–58.
Haas, J.R., Shock, E.L., Sassani, D.C., 1995. Rare earth elements in hydrothermal systems: estimates of standard partial molal thermodynamic properties of aqueous complexes of the rare earth elements at high pressures and temperatures. Geochim. Cosmochim. Acta 59 (21), 4329–4350.
Hedenquist, J.W., Lowenstern, J.B., 1994. The role of magmas in the formation of hydrothermal ore deposit. Nature 370, 519–527.
Irber, W., 1999. The lanthanide tetrad effect and its correlation with K/Rb, Eu/Eu*, Sr/Eu, Y/Ho, and Zr/Hf of evolving peraluminous granite suites. Geochim. Cosmochim. Acta 63 (3), 489–508.
Jebrak, M., Smejkal, V., Albert, D., 1985. Rare earth and isotopic geochemistry of the fluorite–barite vein deposits from the western Rouergue District (France). Econ. Geol. 80 (7), 2030–2034.
Keppler, H., Wyllie, P.J., 1991. Partitioning of Cu, Sn, Mo, W, U, and Th between melt and aqueous fluid in the systems haplogranite–H_2O–HCl and haplogranite–H_2O–HF. Contrib. Mineral. Petrol. 109 (2), 139–150.
Langmuir, D., 1978. Uranium solution–mineral equilibria at low temperatures with applications to sedimentary ore deposits. Geochim. Cosmochim. Acta 42 (6), 547–569.
Lindsey, D.A., 1977. Epithermal beryllium deposit in water-laid tuff, western Utah. Econ. Geol. 72, 219–232.
Ludwig, K.R., 2001. User's Manual for Isoplot/Ex. Version 2.47. A Geochronological Tool for Microsoft Excel. Berkeley Geochronology Center, Berkeley (43p).
Ma, H.F., Yi, L.S., Xiu, X.Q., 2010. Research on evaluation of uranium and beryllium resource potential in Xuemisitan area Xinjiang Uygur Autonomous Region. Intern. Rep. 1–161 (in Chinese with English abstract).
Mao, W., Wang, G., Li, X.F., Wang, M., Xiao, R., 2013. A study of fluid inclusions in Baiyanghe U–Be deposit, Xinjiang. Miner. Depos. 32, 1026–1034 (in Chinese with English abstract).
Mao, W., Li, X.F., Wang, G., Xiao, R., Wang, M., Li, Y.L., Ren, M.C., Bai, Y.P., Yang, F., 2014. Petrogenesis of the Yangzhuang Nb, Ta-rich A-type granite porphyry in the West Junggar, Xinjiang, China. Lithos 198–199, 172–183.
Möller, P., Dulski, P., 1999. LA–ICPMS study of REE and Y distribution in fluorite. Mineral Deposits: Processes to Processingpp. 1133–1136.
Monecke, T., Kempe, U., Monecke, J., 2002. Tetrad effect in rare earth element distribution patterns: a method of quantification with application to rock and mineral samples from granite-related rare metal deposits. Geochim. Cosmochim. Acta 66 (7), 1185–1196.
Monecke, T., Dulski, P., Kempe, U., 2007. Origin of convex tetrads in rare earth element patterns of hydrothermally altered siliceous igneous rocks from the Zinnwald Sn–W deposit, Germany. Geochim. Cosmochim. Acta 71, 335–353.
Monecke, T., Kempe, U., Trinkle, M., Thomas, R., Dulski, P., Thomas, W., 2011. Unusual rare earth element fractionation in a tin-bearing magmatic hydrothermal system. Geology 39 (4), 295–298.
Morozov, M., Trinkler, M., Plötze, M., 1996. Spectroscopic Studies on Fluorites from Li–F and Alkaline Granitic Systems in Central Kazakhstan. Granite-Related Ore Deposits of Central Kazakhstan and Adjacent Areas. Glagol Publishing House, St. Petersburg, pp. 359–369.
Roedder, E., 1984. Fluid inclusions. Rev. Mineral. vol. 12 (646 p.).
Shepherd, T., Rankin, A.H., Alderton, D.H.M., 1985. A Practical Guide to Fluid Inclusion Studies. Blackie, Glasgow 235 pp.
Sheppard, S.M.F., 1981. Stable isotope geochemistry of fluids. In: Rickard, D.T., Wickman, F.E. (Eds.), Chemistry and Geochemistry of Solutions at High Temperatures and Pressures. Physics and Chemistry of the Earth, vol 13 and 14. Pergamon Press, New York, pp. 419–445.
Sheppard, S.M.F., Gilg, H.A., 1996. Stable isotope geochemistry of clay minerals. Clay Miner. Clay Miner. 31, 1–24.
Simon, K., 2001. Does δD from fluid inclusion in quartz reflect the original hydrothermal fluids? Chem. Geol. 177, 483–495.
Steiger, R.H., Jager, E., 1977. Subcommission on geochronology: convention on the use of decay constants in geo- and cosmochronology. Earth Planet. Sci. Lett. 36, 359–362.
Su, Y.P., Tang, H.F., 2005. Trace element geochemistry of A-type granites. Bull. Mineral., Petrol. Geochem. 24, 245–251 (in Chinese with English abstract).
Tang, H.S., Wang, Z.Y., 1998. Late Palaeozoic plate-tectonics and its relationship with copper deposits in northern Junggar, Xinjiang. Miner. Resour. Geol. 64 (12), 91–95.
Tang, G.J., Wang, Q., Wyman, D.A., Li, Z.X., Zhao, Z.H., Jia, X.H., Jiang, Z.Q., 2010. Ridge subduction and crustal growth in the Central Asian Orogenic Belt: evidence from Late Carboniferous adakites and high-Mg diorites in the western Junggar region, northern Xinjiang (west China). Chem. Geol. 277, 281–300.

Taylor Jr., H.P., 1974. The application of oxygen and hydrogen isotope studies to problems of hydrothermal alteration and ore deposit. Econ. Geol. 69, 843–883.
Trinkler, M., Monecke, T., Thomas, R., 2005. Constraints on the genesis of yellow fluorite in hydrothermal barite–fluorite veins of the Erzgebirge, Eastern Germany: evidence from optical absorption spectroscopy, rare-earth-element data, and fluid-inclusion investigations. Can. Mineral. 43 (3), 883–898.
Wang, Z.Y., Tang, H.S., 1997. Major types, ore controlling conditions and ore prospecting perspective of copper deposits in northern Junggar, Xinjiang. Miner. Resour. Geol. 61 (11), 319–324.
Wang, S.L., Wang, D.P., Zhu, X.Y., Wang, J.B., Peng, S.L., 2002. Ore-fluid geochemistry of Tamu-Kala Pb–Zn deposit in Xinjiang. Geol.-Geochem. 30, 34–39.
Wang, M., Li, X.F., Wang, G., Li, Y.L., Shi, Z.L., Lu, K.G., 2012. Geological characteristics of Baiyanghe beryllium–uranium deposits in Xuemisitan volcanic belt, Xinjiang. Miner. Explor. 3, 34–40 (in Chinese with English abstract).
Whalen, J.B., Currie, K.L., Chappell, B.W., 1987. A-type granites: geochemical characteristics, discrimination and petrogenesis. Contrib. Mineral. Petrol. 95, 407–419.
Wood, S.A., 1992. Theoretical prediction of speciation and solubility of beryllium in hydrothermal solution to 300 °C at saturated vapor pressure: application to bertrandite/phenakite deposits. Ore Geol. Rev. 7 (4), 249–278.
Xiao, Y.D., Huang, J.H., Wang, Z., Wang, S.C., Zhou, Y.B., Li, Q.D., 2011. The spatial distribution Be and U orebodies at Baiyanghe deposit, Xinjiang. Explor. Eng. 9, 123–126.
Xiu, X.X., Fan, H.H., Ma, H.F., Yi, L.S., 2011. Hydrothermal alteration and its geochemical characteristics at Baiyanghe U–Be deposit, Xinjiang, NW China. Uranium Geol. 27 (4), 215–222.
Yurimoto, H., Duke, E.F., Papike, J.J., 1990. Are discontinuous chondrite-normalized REE patterns in pegmatitic granite systems the results of monazite fractionation? Geochim. Cosmochim. Acta 54 (7), 2141–2145.
Zhai, W., Sun, X.M., He, X.P., Su, L.W., Wu, Y.L., Dong, Y.X., 2007. Geochemistry of ore forming fluid and mechanism of Axi low sulfidation gold deposit in Xinjiang, China. Acta Geol. Sin. 81, 659–669.
Zhang, X., Zhang, H., 2014. Geochronological, geochemical, and Sr–Nd–Hf isotopic studies of the Baiyanghe A-type granite porphyry in the Western Junggar: implications for its petrogenesis and tectonic setting. Gondwana Res. 25, 1554–1569.
Zhao, Z.H., Bao, Z.W., Qiao, Y.L., 2010. A special "M" and "W" composite REE tetrad effect — the case study for Shuiquangou complex. Chin. Sci. Bull. 15, 1474–1488.
Zheng, Y.F., 1993. Calculation of oxygen isotope fraction in hydroxyl-bearing silicates. Earth Planet. Sci. Lett. 120 (3–4) (247–260).
Zou, T.R., 2006. REE and Rare Metal Deposits in Xinjiang, China. Geological Publishing House, Beijing p. 284.